CITATION

DOI

COPYRIGHT

USAGE

# Regional Rainfall Measurements

## Using the Passive Aquatic Listener
## During the SPURS Field Campaign

By Jie Yang, Stephen C. Riser,
Jeffrey A. Nystuen, William E. Asher,
and Andrew T. Jessup

>> ...passive acoustic remote sensing can be used to understand the spatial variability and intermittency of rainfall and to provide regional maps of the surface wind field, both of which will advance understanding of the freshwater budget at the ocean surface and its impact on the global water cycle. <<

**ABSTRACT.** Knowledge of the intensity and spatial-temporal distribution of rainfall over the ocean is critical in understanding the global hydrological cycle. However, rain has proven difficult to measure over the ocean due to problems associated with platform motion and flow distortion combined with the spatial and temporal variability of rainfall itself. Underwater acoustical rain gauges avoid these issues by using the loud and distinctive underwater sound generated by raindrops on the ocean surface to detect and quantify rainfall. Here, the physics and operation of and results from an instrument that uses underwater ambient sound to measure rainfall rate and wind speed are presented. Passive Aquatic Listener (PAL) instruments were mounted on a buoy deployed at Ocean Station P and on 13 Argo profilers that were deployed as part of the US National Aeronautics and Space Administration-sponsored Salinity Processes in the Upper-ocean Regional Study (SPURS) field experiment in the North Atlantic Ocean. The PALs provide near-continuous measurements of rain rate and wind speed during the two-year period over the SPURS study region defined by the Argo profilers. Comparisons of PAL data with rain and wind measured by other techniques, including direct in situ observations and satellite measurements, show good agreement for both rain rate and wind speed.

## INTRODUCTION

The water cycle is an important component of global climate, and its variability is tightly correlated with climate variability. The two most important processes in the global water cycle are evaporation and precipitation, with the ocean being the largest source of water to the atmosphere (i.e., 90% of global freshwater flux to the atmosphere is the result of evaporation from the ocean surface). Similarly, the ocean is also the largest recipient of freshwater from the atmosphere, with 80% of the total global precipitation delivered to the ocean surface.

Freshening of the ocean surface due to rain is evident in global maps of sea surface salinity (SSS), where areas with high precipitation are broadly coincident with areas of low salinity, and regions of high salinity occur in regions with low precipitation and high evaporation. Transfer of water from evaporating regions to precipitating regions is a principal component of the global water cycle and drives much of the large-scale circulation of the atmosphere. In addition to atmospheric effects, rain is also a key component in ocean circulation through its effect on ocean surface density (density gradients are among the primary drivers of ocean circulation). Seawater density is determined by temperature and salinity, and freshwater input to the ocean surface from rain causes density gradients. These gradients affect vertical mixing and horizontal advection in the ocean surface mixed layer over a range of spatial and temporal scales.

Measurement of rainfall at sea is problematic: platform motion and flow distortion around the platform can affect surface-based sensors such as in situ gauges, tipping buckets, and disdrometers (Quartly et al., 2002). In addition, research vessels and other manned platforms that support rain sensors generally do not stay on station long enough to monitor rainfall trends longer than several weeks, making it difficult to observe variability over interannual, seasonal, or monthly times scales. Surface rain gauges mounted on unattended buoys are often vandalized, leading to loss of data. In order to reduce these problems, satellite-based rain-monitoring instruments such as the Tropical Rainfall Measuring Mission (TRMM) or the Global Precipitation Mission (GPM) are used to measure rain rates over the ocean. TRMM produces rainfall data with three-hour temporal resolution and $0.25° \times 0.25°$ spatial resolution in a global belt extending from 50°S to 50°N latitude. Although TRMM measures precipitation with unprecedented spatial resolution, the three-hour repeat time likely does not capture the full temporal variability, given what we know about the time scales of rainfall over the ocean. Measuring rain using submerged acoustic rain gauges provides a method that is essentially vandalism-proof, can provide spatial resolution comparable to TRMM, but with temporal resolution on order of a few minutes and deployment times of years. This paper describes a state-of-the-art acoustic rain gauge, the Passive Aquatic Listener (PAL), which is currently deployed on selected Argo

profiling drifters to measure rain over the North Atlantic Ocean during the first field experiment for the Salinity Processes in the Upper-ocean Regional Study (SPURS) field program (SPURS-1).

## WORKING MECHANISM

The underwater ambient sound field consists of sound produced biologically (e.g., marine mammals, snapping shrimp), anthropogenically (e.g., shipping), and geophysically (e.g., rainfall, wind). Acoustic detection and quantification of rain rate and wind speed have been developed through both laboratory and field studies. As part of this development effort, prototype and experimental devices have been in use for several decades in numerous field programs (Shaw et al., 1978; Pumphrey et al., 1989; Medwin et al., 1990, 1992; Nystuen and Medwin, 1995; Nystuen, 1986, 1993; Nystuen and Selsor, 1997).

The Passive Aquatic Listener acoustic rain gauge has been developed by the Applied Physics Laboratory at the University of Washington (APL-UW) for making routine measurements of rain rate and wind speed over the ocean. A PAL consists of a broadband, low noise hydrophone, control electronics for data collection/signal processing, and a battery pack. Typically, it records a 4.5-s-long time series of sound pressure and converts it to a frequency spectrum of sound pressure levels (SPL) over the frequency range of 1–50 kHz. The spectrum is then sampled at eight discrete frequencies (1, 2, 5, 8, 15, 20, 30, and 40 kHz) and averaged over a 1 kHz bandwidth. These discrete values are used to classify the spectra to determine the dominant noise source. Once the noise source is identified, and assuming the source is found to be either wind or rain, the SPLs at specific frequencies can then be used to estimate wind speed or rain rate, respectively. Collecting sequential SPL records forms a time series for rain rate and wind speed. PAL is adaptive in terms of data collection, and the sampling rate for spectra collection can be adjusted depending on the source of the acoustic signal and mission requirements. For example, the sampling rate is normally set to measure one SPL spectrum every eight minutes. This rate increases to one SPL spectrum every two minutes when rainfall is detected.

The area sampled by PAL depends on the directivity beam pattern of the ambient noise field. In an open-ocean scenario with deep water and no reflection path from the seafloor to the sensor, sound only comes from the sea surface. Therefore, the received SPL signal is the sound pressure that is spatially averaged over a circular area above the instrument. In this situation (i.e., no reflection from the seafloor), the spectral quantities of the received sound are independent of instrument depth. In general, for the hydrophone used in PAL, the effective listening radius is approximately two to three times the deployment depth so that when deployed at a depth of 1 km, a PAL averages over a circular area approximately 5 km in diameter. This footprint is approximately the same size as the footprint of the precipitation radar on TRMM.

In the frequency range of 1–50 kHz, the dominant ambient noise sources are rain, wind, and breaking waves, although sound from shipping and marine mammals can make significant contributions to the measured SPLs. Therefore, the first step in data analysis is to classify the dominant noise source for each spectrum and then exclude data records contaminated by biological or anthropogenic sources. As Figure 1a shows, each noise source has a distinct spectral shape in terms of SPL at a particular frequency and in the slopes between the SPLs at different frequencies.
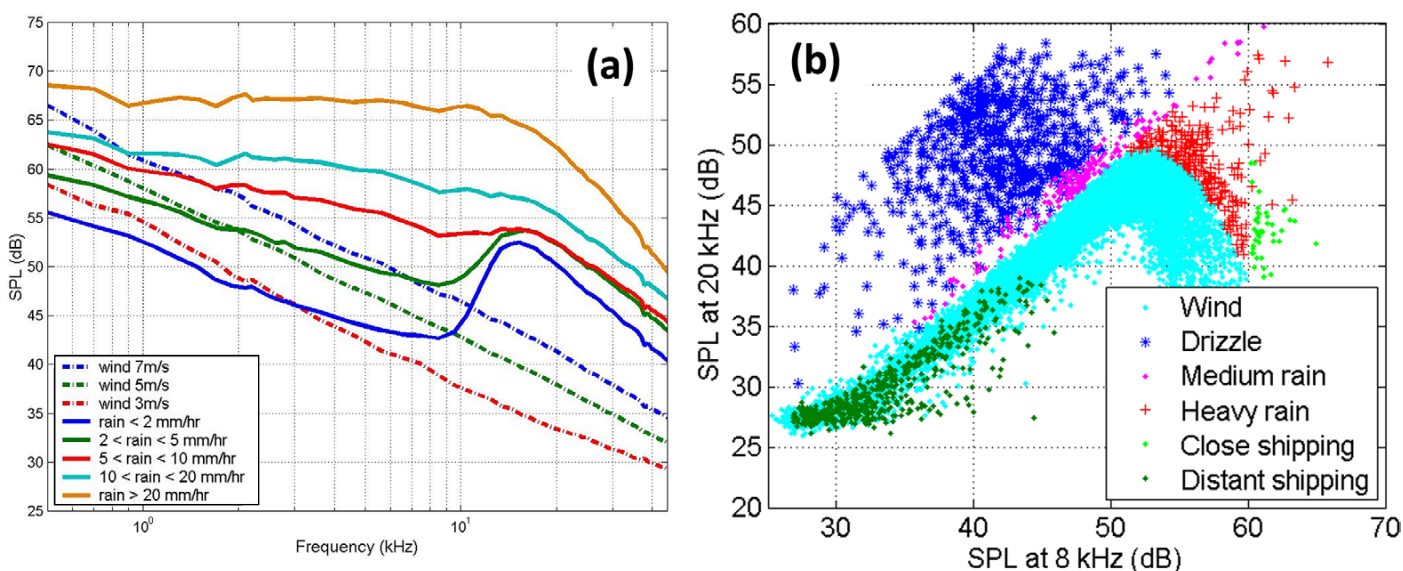


**FIGURE 1.** (a) Ambient sound spectra from three wind speed categories and five rainfall rate categories (Ma and Nystuen, 2005). These data are from Passive Aquatic Listener (PAL) deployments in the Intertropical Convergence Zone (ITCZ) of the eastern tropical Pacific Ocean. (b) Classification diagram using sound pressure levels (SPLs) at 8 kHz and 20 kHz for light rain transitioning to heavy rain, wind only, and distant to close shipping noise.

These characteristics are used to classify a measured, discretized spectrum in terms of its dominant source.

In particular, numerical thresholds are defined for SPL levels and slopes for each noise source based on SPL calibration curves such as shown in Figure 1a, where SPL levels were measured for known noise sources. Figure 1b shows an example of a classification diagram using the SPL at 8 kHz and 20 kHz. In this figure, when the SPL at 8 kHz is plotted versus the SPL at 20 kHz, light drizzle, medium rain, heavy rain, distant ship noise, and nearby ship noise fall into specific regions of the plot (with the exception of wind and distant shipping, which tend to overlap at these two frequencies; Nystuen et al., 2011). Therefore, the ratio of SPLs at 8 kHz and 20 kHz and their absolute levels form the starting test in the overall classification scheme, and additional tests are used to validate the initial sorting (and to separate distant shipping noise from wind-dominated cases). Figure 1b also shows how in the case of wind-generated noise, the two sound levels in general increase in proportion to each other as wind speed increases (which is equivalent to noting that increasing wind speed correlates with increasing sound level). However, the data also show that this correlation breaks down at high wind speed, where the SPL at 20 kHz rises to a peak value as the SPL at 8 kHz increases, and then decreases as the SPL at 8 kHz increases further. This transition occurs when wind speed exceeds about 10 m s$^{-1}$, which is significant because there is also the onset of significant large-scale wave breaking with bubble entrainment at this wind speed.

### PAL CALIBRATION

A PAL was deployed in the North Pacific from 2007–2012 at Ocean Station P (OSP), one of the National Oceanic and Atmospheric Administration's Ocean Climate Stations (NOAA-OCS) and the site of a buoy instrumented with the NOAA-OCS standard meteorological instrument package (http://www.pmel.noaa.gov/OCS/technology/sensors.html). The package includes wind speed measured by a Gill Windsonic ultrasonic anemometer and precipitation measured using an RM Young Model 50203-34 capacitance rain gauge. Data from these sensors were downloaded from the NOAA-OCS website at http://www.pmel.noaa.gov/OCS/data/asciidata.html. Rain rate and wind speed are available as 10-minute averaged quantities. These in situ data can be compared with corresponding PAL-derived quantities.

Figure 2 shows a spectrogram of two days of SPL data for February 11–12, 2008. The time series show distinct periods when three separate sound sources are identified. For light rain (i.e., raindrops <2 mm in diameter), the splash from a droplet's impact generates bubbles that resonate between 13 and 20 kHz, allowing light rain to be easily identified (Pumphrey et al., 1989; Oguz and Prosperetti, 1990; Longuet-Higgins, 1990). Heavy rain with larger raindrops generates turbulent splashes that also entrain bubbles, but there are at least two different bubble entrainment mechanisms for large raindrops, which cause the bubbles for large raindrops to vary widely in size (Nystuen and Medwin, 1995). Specifically, the two mechanisms correspond to bubble generation from (1) direct impact of raindrops, and (2) secondary splashes of airborne drops thrown up by the initial impact. This change in bubble size spectrum causes the acoustic signal from large raindrops to spread over a wide frequency range (1–50 kHz) compared to light rain. Drop size inversion results are also plotted in Figure 2 for small (<2 mm), medium (2–3 mm), and large (>3 mm) drop sizes (Nystuen, 2001). For light rain, mostly small raindrops are observed, while large to extra-large raindrops are only be observed during heavy rain. In the absence of rain, the overall sound intensity is highly correlated with wind speed (black curve in Figure 2, which explains how wind speed can be measured accurately using PAL.

Once each SPL spectra is classified as dominated by either wind or rain (with spectra containing ship or biological noise discarded), the SPL values at different frequencies can be used to estimate
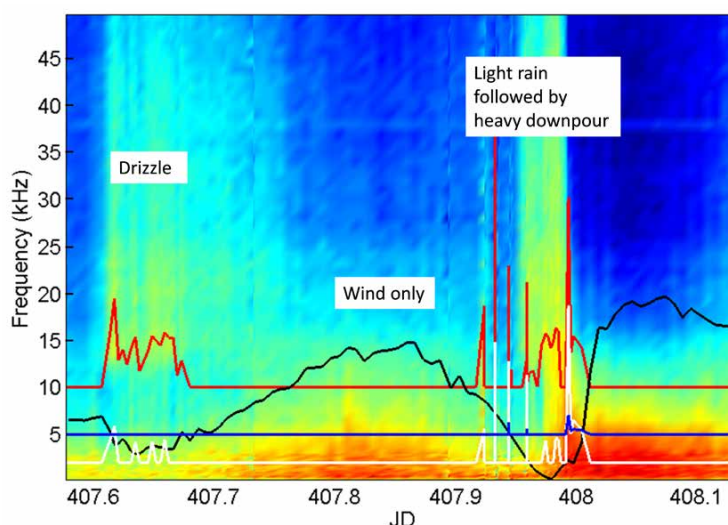


**FIGURE 2.** Spectrogram of ambient sound recorded by PAL at Ocean Station P from February 11 to February 12, 2008. Three time periods of light rain (drizzle), wind only, and light rain followed by heavy rain are identified. Black indicates wind speed from National Oceanic and Atmospheric Administration (NOAA) Ocean Station P buoy data (range 0–22 m s$^{-1}$). The red, white, and blue curves show small (i.e., diameter<2 mm), medium (i.e., 2 mm<diameter<3 mm), and large (i.e., diameter>3 mm) raindrop size inversion results, respectively.
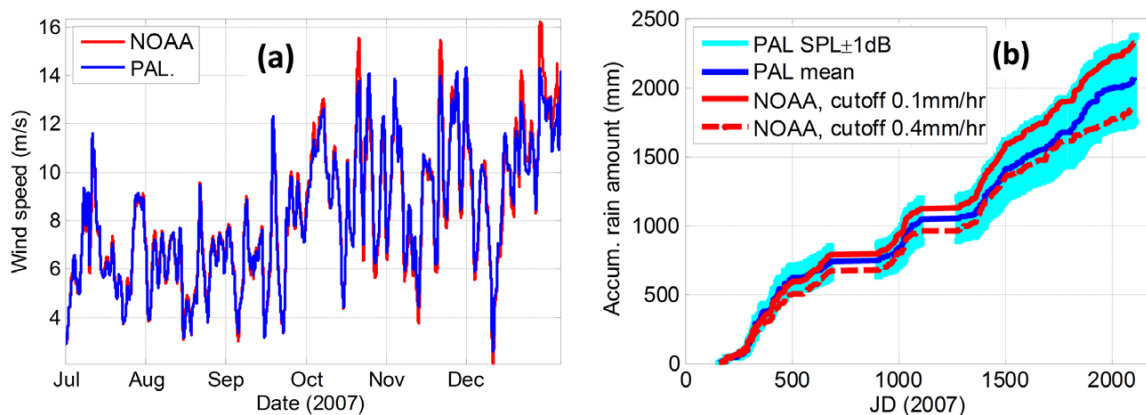
**FIGURE 3.** Comparison between PAL and NOAA buoy data collected at Ocean Station P for (a) wind speed, and (b) total accumulated rain from 2007 to 2012. In (b), the background cyan curve shows the uncertainty bounds of PAL estimates, and the blue is its mean curve. Because NOAA buoy data show clear noise, including negative rain rates, the data were cut off at 0.1 mm h$^{-1}$ and 0.4 mm h$^{-1}$ to calculate total rain amount to compare with PAL.

wind speed or rainfall. In the case of wind speed, it is known that SPL spectra associated with wind result from resonant acoustic radiation from bubbles generated by breaking waves (Medwin and Beaky, 1988). The population size distribution of the bubbles defines the shape of the SPL spectra, and this shape of distribution is invariant with wind speed. However, as wind speed increases, the total bubble concentration increases because the fractional area coverage of breaking waves increases. The increase in bubble concentration leads to a concomitant increase in the SPL across all frequencies. This uniform increase as a function of frequency allows the SPL at a single frequency to be used to estimate wind speed (Vagle et al., 1990). The algorithm from Vagle et al. (1990) based on the SPL at 8 kHz is used to extract wind speed from PAL SPL spectra. Figure 3a shows the comparison between wind speed estimated acoustically and measured by the anemometer mounted on the NOAA-OCS buoy deployed at OSP for the time period July to December 2007. In general, the agreement is excellent except for wind speed >15 m s$^{-1}$, where PAL-measured winds are less than the buoy measurements. This bias is due to the absorption of sound energy by bubbles that have been advected downward from the ocean surface at high wind speeds.

For data that have been classified as rain, the SPL at 5 kHz is used to quantify rain rate using the relationship

$$R = 10^{((SPL_5 - 42.4)/15.4)}/2$$

where $R$ is rain rate in mm h$^{-1}$ and $SPL_5$ is the SPL at 5 kHz in dB (Ma and Nystuen, 2005; Nystuen et al., 2008). This formula is applied to the OSP data recorded by the PAL from June 2007 to October 2012. The total rain accumulation (RA in mm) can be compared with rain data acquired by the in situ rain gauge mounted on the NOAA-OCS OSP buoy. Figure 3b compares rain accumulation measured by the PAL and by the in situ gauge. The blue curve is rain accumulation from the PAL. The cyan shading shows the range in rain accumulation measured by the PAL, assuming there is a ±1 dB uncertainty in SPL (which is a result of uncertainty in hydrophone receiver sensitivity).

Turning to the comparison of rain measured by the in situ rain gauge and PAL, rain rate from the in situ rain gauge showed considerable noise, including negative values for rain rate. This is typical for rain rates derived from accumulation data from a capacitance rain gauge over relatively short time intervals. The negative rain rates correspond to noise in the data, where the apparent decreases in the reservoir volume due to sloshing in the gauge (and to a much lesser extent from

evaporation from the reservoir between rain events) cause the calculation procedure to produce a negative rain rate. Therefore, two different thresholds for accepting a valid rain rate from the in situ gauge are shown in Figure 3b to provide an estimate of the uncertainty in the surface measurement. The lower threshold of rain rate, 0.1 mm h$^{-1}$, represents the lowest rain rate that can be measured by the in situ gauge. The noise band of the in situ gauge defines the upper threshold of rain rate of 0.4 mm h$^{-1}$.

In Figure 3b, rain accumulation from PAL lies between the two estimates of accumulated precipitation provided by the in situ gauge. The agreement in rain accumulation between the two measurements provides evidence that measuring rain rate using the PAL provides an accurate estimate of rainfall over the ocean. However, the large range shown by the cyan shading in Figure 3b makes it clear that better calibration of the PAL sensor is needed. This would reduce the uncertainty in hydrophone sensitivity, which is the dominant source of uncertainty in PAL measurements. For example, reducing the uncertainty in SPL to ±0.5 dB by in situ calibration of each PAL would lead to a reduction in the error band shown in cyan in Figure 3b by a factor of two.

The six-year-long record provided by the OSP data set, which includes rain

measured by both PAL and the in situ gauge, can be used to compare rainfall climatology for both instruments. Figure 4 shows a six-month time series of rain rate from each sensor. In general, PAL and the in situ rain gauge are in near perfect agreement in identifying the presence of rain. However, rain rate measured by PAL is in general higher than that from the in situ gauge, which results from a difference in averaging time for the two instruments. Rain rate from PAL is near-instantaneous measurement of rain rate made every two minutes. In contrast, rain rate from the in situ gauge is calculated from 10-minute averages of rain accumulation, leading to a decrease in the measured rain rate compared to PAL data. However, as Figure 3b and Table 1 show, accumulated precipitation agrees between the two techniques over the entire time period.

Table 1 summarizes the rain statistics for both PAL and the in situ gauge using a threshold of rain accumulation of >3 mm to identify rain events. When this threshold is used to segment each data set, the total number of rain events, the percentage time raining, and the total accumulated rainfall are in good agreement between PAL and the in situ gauge. Table 1 also shows the number of rain events observed by PAL and the in situ gauge that are coincident in time, indicating that PAL identifies 70% of the rain events detected by the in situ gauge, which accounts for 75% of the rain accumulation.

**TABLE 1.** Comparison of rain climatology between a Passive Aquatic Listener (PAL) deployed at Ocean Station P (OSP) and an in situ rain gauge mounted on the NOAA-Ocean Climate Station buoy at OSP derived from the total six-year data record from each instrument. Data were recorded from January 2007 through November 2012.

| | # Rain Events (RA >3 mm) | % Time Raining | Rain Accumulation (RA) (mm) |
|---|---|---|---|
| PAL | 173 | 10% | 1,515 |
| NOAA | 207 | 13% | 1,486 |
| Overlapping Events | 142 | – | PAL: 1,340 NOAA: 1,130 |

The passive acoustic technique presented here has several advantages over conventional meteorological buoy measurements, including that the instrument is autonomous and low cost, has long residence time at sea, transmits real-time data using data telemetry, and provides excellent temporal and spatial resolutions. PAL has been established to provide reliable estimates of wind speed and rain rate.

## PAL DEPLOYMENTS IN SPURS-1

The objectives of SPURS-1 are to understand and quantify the processes that control salinity in an ocean region where the loss of freshwater from the surface through evaporation is larger than the input of freshwater from rainfall. Measurement of rain over the study area is a key component of the SPURS-1 measurements because, in this region, rain is the sole freshwater input to the ocean surface. However, the spatial heterogeneity of rain makes it difficult to estimate total rainfall over a study region as large as that of SPURS-1 from a single point measurement. The deployment of an array of PALs mounted on Argo profiling drifters allows measurement of rain over a much broader area than is feasible using traditional rain gauges.

## Rain Rate and Wind Speed Results During SPURS-1

PALs have been incorporated into Argo profilers since 2004 and have been deployed in the Bay of Bengal (Riser et al., 2008), the equatorial Pacific (Anderson and Riser, 2014), and as part of SPURS-1 in the North Atlantic. The PALs measure wind speed and rain rate while the floats are drifting at their parked depths (typically 1 km). The position of each float is recorded about every 10 days when it surfaces as part of its profiling operation.

During SPURS-1, a total of 13 floats equipped with PALs were deployed in September 2012 to provide rain and wind speed over the duration of the experiment. Figure 5a shows the starting positions of the floats as indicated by the black circles. The profilers were initially deployed in a rectangular array within a 2° × 2° box. The gray lines in Figure 5a depict float trajectories from September 2012 to March 2014. The light gray dots on each float trajectory represent the points where the float surfaces. The red circles show the ending positions of the floats. There was a maximum 8° (~800 km) drift over the 1.5 year SPURS-1study period, so the final array covered a 7° × 10° box.

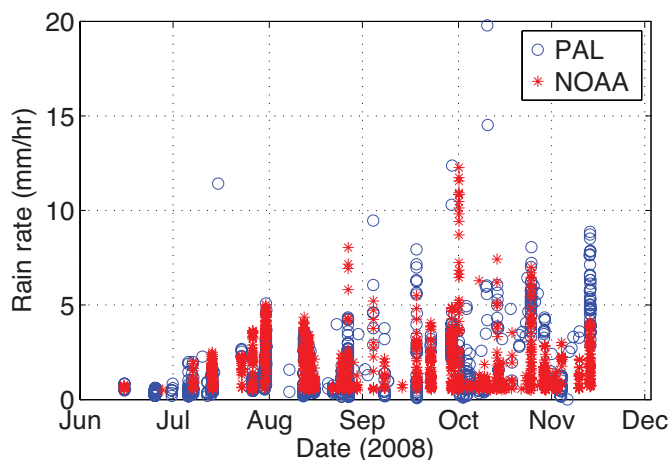Following the classification procedure described above, the recorded SPL



**FIGURE 4.** Comparison of six months of rain rates measured by a PAL deployed at Ocean Station P and by an in situ rain gauge mounted on the NOAA-Ocean Climate Station buoy at Ocean Station P.

spectra were sorted into rain-, wind-, or other noise-source-dominated categories. The wind-dominated spectra provide a time series of wind speeds measured by PAL that can be compared with wind speed measured by an anemometer mounted on the SPURS-1 central mooring (see Figure 5b). In general, the two wind speed data sets are in good agreement, especially considering that the PAL is separated from the buoy by a distance of approximately 200 km. In agreement with the OSP results presented above, Figure 5b shows that PAL provides accurate estimates of wind speed over the SPURS-1 study area.

For the SPL spectra where the noise was classified as rain dominated, rain rate was calculated using $SPL_5$, as described above. Rain accumulation was then calculated from rain rate by integrating the time series of rain rate with respect to time. Figure 6 shows rain accumulation from four representative PALs deployed during SPURS-1 on Argo profilers 7547, 7582, 7587, and 7607 (final positions identified in Figure 5a). The background blue curve is the PAL rain accumulation with ±1 dB SPL uncertainty, and the red curve is its mean. The data demonstrate the spatial heterogeneity of rainfall over the study area. For example, the final value for accumulated precipitation

for float 7547 (Figure 6a) is a factor of two less than the final accumulated precipitation for float 7587 (Figure 6c), with the final positions of the two separated by 800 km. However, the total rain accumulation for float 7582 (Figure 6b), float 7587 (Figure 6c), and float 7607 (Figure 6d) are in reasonable agreement even though they are separated by similar amounts to the separation between 7547 and 7587.

The PAL-derived rain data were compared with the NASA 3B42 V7 rain data product (hereafter referred to as 3B42). The 3B42 data set is derived from TRMM measurements and provides rain rate and rain accumulation at 3 h intervals with 0.25° × 0.25° spatial resolution. Accumulated precipitation was extracted from 3B42 on a 0.5° × 0.5° grid over the entire SPURS region (22°–29°N and 29°–42°W). Because the PAL rain rates represent a time series that is sampled at different locations as the Argo profilers drift and the 3B42 data are available every three hours at times that are not necessarily coincident with the PAL data, it is not possible to directly compare the PAL rain data with the grid extracted from the 3B42 archive. Therefore, a time series of data from the 3B42 grid that is spatially and temporally coherent with each PAL was constructed by linearly interpolating

spatially and temporally along the trajectory and rain sampling times of each float onto the 3B42 data grid.

Figure 6 also compares rain accumulation from February 1, 2013, to February 1, 2014, between PAL and 3B42. The 3B42 data are shown in magenta, and in general lie within the uncertainty bounds (i.e., the blue shaded region) of the PAL results. The step increases in rain accumulation represent major rain events and are coincident between PAL and 3B42. However, the change in rain accumulation is not identical in some cases. These differences might be caused by fundamental differences in the measurements between the two techniques. One possibility is that the difference in sample area (i.e., the sampling radius for PAL is a few kilometers versus the 25 km spatial scale of the 3B42 data set) leads to differences because of small-scale variability in the rain field. PAL also provides a near-instantaneous measurement of rain rate versus the 3 hr average provided by 3B42. Detailed analysis of this issue is the subject of further research.

### Rainfall Seasonal and Intra-Annual Variability in the SPURS Region
Of the 13 PAL-equipped Argo profilers deployed during SPURS-1 in September 2012, 10 PALs are still recording data in
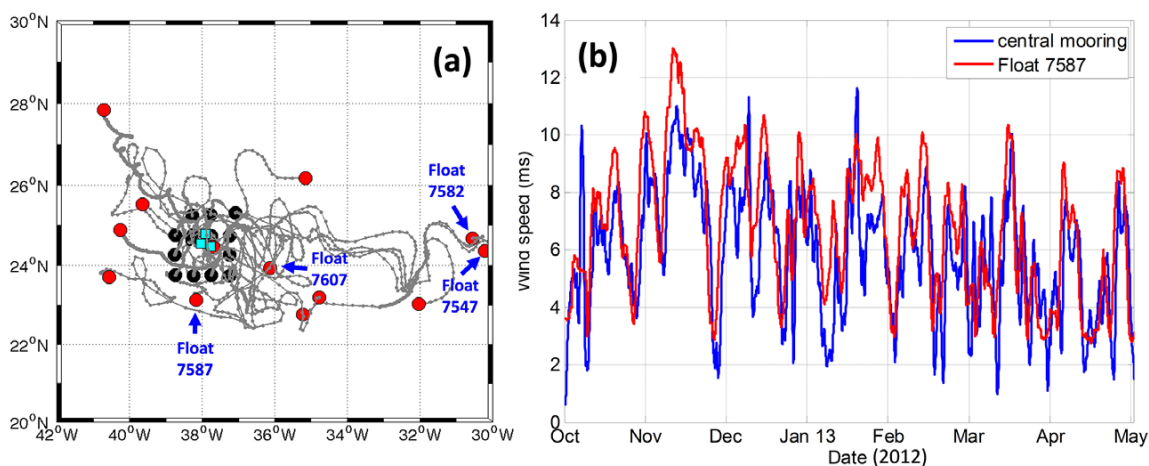


**FIGURE 5.** (a) Argo float trajectories recorded during Salinity Processes in the Upper-ocean Regional Study (SPURS) work, with float 7587 highlighted. Black and red circles indicate the starting and ending positions of each float. *Courtesy of Jessica Anderson* (b) Comparison of acoustically derived wind data speed from float 7587 with buoy measurements at the central mooring location, ~200 km apart.

the SPURS-1 region. Rain rate from these 10 instruments can be used to study the seasonal and intra-annual variability of rain in that region from September 2012 to July 2014. First, the total time series of rain rate from each PAL was separated into two parts: September 2012 to August 2013 and September 2013 to July 2014. Then, the rain accumulation data from all instruments were combined to form a regional estimate of rain rate. Figure 7a shows rain rate from all 10 floats in the first full year, and Figure 7b shows rain rate from the second partial year. In both years it is clear that September to March is the rainy season while April to August is the dry season. Most rain events are characterized by R < 10 mm hr$^{-1}$, but there are approximately 10 rain events over the annual cycle in 2012–2013 that registered R > 20 mm hr$^{-1}$. In the following year, 2013–2014, although data are missing for July and August, the total rainfall is less and the dry season starts about one month earlier than the previous year. These data show the inter-annual variability in rainfall, although a longer record is required to understand which case represents the departure from a mean rainfall pattern.

## Implication of Rainfall Measurements on Salinity

Given that the goal of SPURS-1 is to understand the formation of the high-salinity water that is characteristic of the study area, the PAL rain data can be used to determine if, in a general sense, annual changes in regional salinity are correlated with the rainfall patterns observed in Figure 7. If rain is an important component of the surface salinity budget, then a decrease in surface salinity might be expected during the rainy season when the freshwater input is greatest. Conversely, salinity should increase during the dry season. As an initial test of this hypothesis, Figure 8 shows sea surface salinity, S (‰), measured at 0.86 m below the ocean surface on the SPURS-1 central mooring from September 2012 until its recovery in September 2013. Figure 8
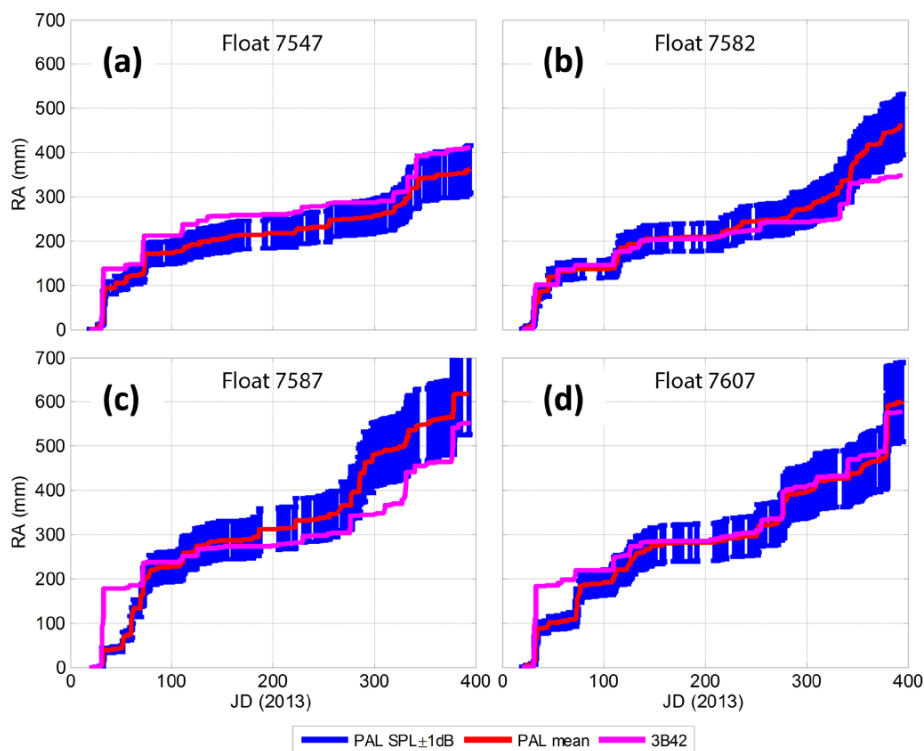


**FIGURE 6.** Comparison of rain accumulation between PAL and Tropical Rainfall Measuring Mission (TRMM) 3B42 from February 1, 2013, to February 1, 2014, for floats (a) 7547, (b) 7582, (c) 7587, and (d) 7607. Background blue curve = acoustic accumulated precipitation with ±1 dB SPL uncertainty. Red = mean acoustic accumulated precipitation. Magenta = TRMM 3B42 data interpolated along the float trajectory.
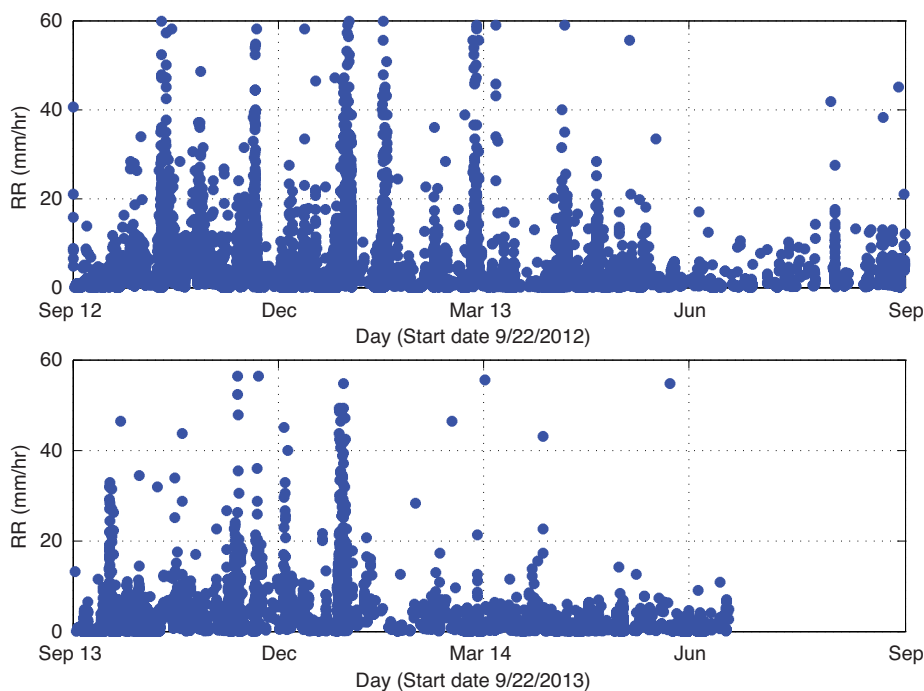


**FIGURE 7.** Seasonal and intra-annual variability in rainfall during SPURS. (a) Combined rain rate time series from 10 floats from September 2012 to September 2013, and (b) combined rain rate time series from the same 10 floats from September 2013 to July 2014.

also shows a composite 10-day average rain rate computed from the rain rate data in Figure 7a. The composite average rain rate was computed by first calculating the mean rain rate from the 10 PALs and then using that mean rate to calculate a 10-day running average rain rate.

Because September is the end of the dry season and freshwater input is at the annual minimum, Figure 8 shows that salinity is high, as might be expected. As the rainy season starts in October and progresses through December, salinity decreases and remains low until June, when the dry season begins. Salinity then starts to increase and recovers to the previous year's level. It is interesting that the salinity change is not instantaneous but rather lags the rainfall by about one to two

months. For example, during October to November 2012 (YD 275–335), salinity remains constant, although rain rate increases. However, there is a sharp drop of 0.2 in salinity over the span of about 10 days during the large maximum in rain rate from YD 360 to YD 400. In addition, at the end of the rainy season (around May, YD 500), there is a slight decrease in salinity even in the absence of significant rainfall. Lateral advection and vertical mixing are possible explanations for the lack of correlation between rainfall and salinity.

## SUMMARY AND FUTURE

The long-term goal of this research is to use passive acoustic remote sensing of the marine environment as a standard

measurement technique for observing air-sea interaction processes. This work builds on the existing understanding of oceanic sound generation mechanisms for rain, wind, wave breaking, marine mammals, and shipping. As shown above, passive acoustic remote sensing can be used to understand the spatial variability and intermittency of rainfall and to provide regional maps of the surface wind field, both of which will advance understanding of the freshwater budget at the ocean surface and its impact on the global water cycle.

Specifically, PALs have been deployed on deepwater moorings and on Argo floats and have been shown to provide high-quality rain and wind data sets. The six-year-long calibration data set from Ocean Station P establishes that this passive acoustic technique can characterize the underwater ambient sound field. The details of the sound spectra can be used to classify noise sources and quantify rain and wind at the ocean surface.

When deployed on Argo profiling drifters over a larger region as was done in SPURS-1, multiple PALs have been shown to provide an unprecedented data set of regional rainfall patterns over the ocean. When combined with data that characterize vertical and horizontal advection of water in the region, the rain fields provided by the PAL array will be useful in understanding small-scale spatial and temporal variability in surface salinity. ☯
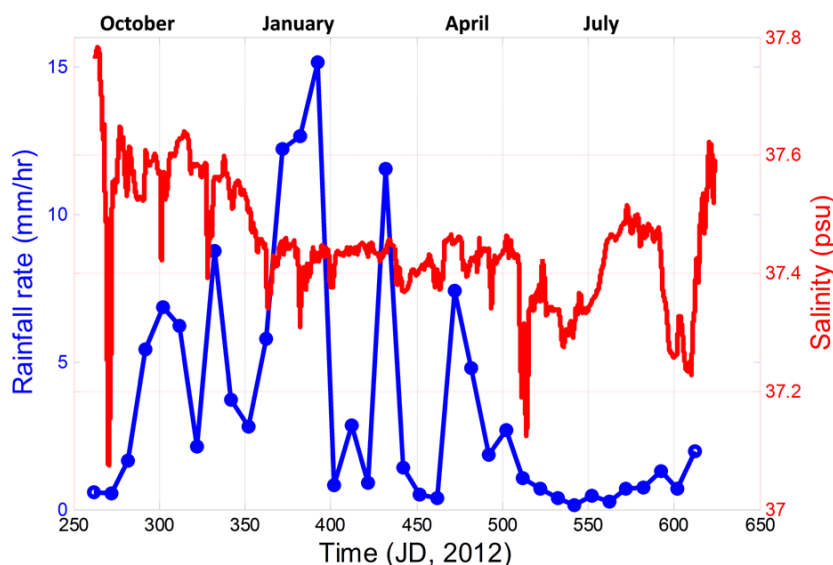


**FIGURE 8.** Comparison of 10-day averaged rain rate results from 10 floats (blue) with salinity measured on the central mooring (red) during SPURS from September 18, 2012 to September 15, 2013.

## REFERENCES

Anderson, J., and S. Riser. 2014. Near-surface variability of temperature and salinity in the near-tropical ocean: Observations from profiling floats. *Journal of Geophysical Research* 119:7,433–7,448, http://dx.doi.org/10.1002/2014JC010112.

Longuet-Higgins, M.S. 1990. An analytic model of sound production by raindrops. *Journal of Fluid Mechanics* 214:395–410, http://dx.doi.org/10.1017/S0022112090000179.

Ma, B., and J.A. Nystuen. 2005. Passive acoustic detection and measurement of rainfall at sea. *Journal of Atmospheric and Oceanic Technology* 22:1,225–1,248, http://dx.doi.org/10.1175/JTECH1773.1.

Medwin, H., and M.M. Beaky. 1988. Bubble sources of the Knudsen sea noise spectra. *Journal of the Acoustical Society of America* 86:1,124–1,130, http://dx.doi.org/10.1121/1.398104.

Medwin, H., A. Kurgan, and J.A. Nystuen. 1990. Impact and bubble sound from raindrops at normal and oblique incidence. *Journal of Acoustical Society of America* 88:413–418, http://dx.doi.org/10.1121/1.399918.

Medwin, H., J.A. Nystuen, P.W. Jacobus, L.H. Ostwald, and D.E. Synder. 1992. The anatomy of underwater rain noise. *Journal of the Acoustical Society of America* 92:1,613–1,623, http://dx.doi.org/10.1121/1.403902.

Nystuen, J.A. 1986. Rainfall measurements using underwater ambient noise. *Journal of the Acoustical Society of America* 79:972–982, http://dx.doi.org/10.1121/1.393695.

Nystuen, J.A. 1993. An explanation of the sound generated by light rain in the presence of wind. Pp. 659–668 in *Natural Physical Sources of Underwater Sound.* B.R. Kerman, ed., Kluwer Academic Publishers.

Nystuen, J.A. 2001. Listening to raindrops from underwater: An acoustic disdrometer. *Journal of Atmospheric and Oceanic Technology* 18:1,640–1,657, http://dx.doi.org/10.1175/1520-0426(2001)018<1640:LTRFUA>2.0.CO;2.

Nystuen, J.A., E. Amitai, E.N. Anagnostou, and M.N. Anagnostou. 2008. Spatial averaging of oceanic rainfall variability using underwater sound: Ionian Sea Rainfall Experiment 2004. *Journal of the Acoustical Society of America* 123:1,952–1,962, http://dx.doi.org/10.1121/1.2871485.

Nystuen, J.A., and H. Medwin. 1995. Underwater sound generated by rainfall: Secondary splashes of aerosols. *Journal of the Acoustical Society of America* 97:1,606–1,613, http://dx.doi.org/10.1121/1.412099.

Nystuen, J.A., S.C. Riser, T. Wen, and D. Swift. 2011. Interpreted acoustic ocean observations from Argo floats. *Journal of the Acoustical Society of America* 129:2,400, http://dx.doi.org/10.1121/1.3587814.

Nystuen, J.A., and H.D. Selsor. 1997. Weather classification using passive acoustic drifters. *Journal of Atmospheric and Oceanic Technology* 14:656–666, http://dx.doi.org/10.1175/1520-0426(1997)014<0656:WCUPAD>2.0.CO;2.

Oguz, H.N., and A. Prosperetti. 1990. Bubble entrainment by the impact of drops on liquid surfaces. *Journal of Fluid Mechanics* 218:143–162, http://dx.doi.org/10.1017/S0022112090002890.

Pumphrey, H.C., L.A. Crum, and L. Bjorno. 1989. Underwater sound produced by individual drop impacts and rainfall. *Journal of the Acoustical Society of America* 85:1,518–1,526, http://dx.doi.org/10.1121/1.397353.

Quartly, G.D., T.H. Guymer, and K.G. Birch. 2002. Back to basics: Measuring rainfall at sea: Part 1. In situ sensors. *Weather* 57:315–320.

Riser, S.C., J.A. Nystuen, and A. Rogers. 2008. Monsoon effects in the Bay of Bengal inferred from profiling float-based measurements of wind speed and rainfall. *Limnology and Oceanography* 53(5, part 2):2,080–2,093, http://dx.doi.org/10.4319/lo.2008.53.5_part_2.2080.

Shaw, P.T., D.R. Watts, and H.T. Rossby. 1978. On the estimation of oceanic wind speed and stress from ambient noise measurements. *Deep Sea Research* 25:1,225–1,233, http://dx.doi.org/10.1016/0146-6291(78)90015-2.

Vagle, S., W.G. Large, and D.M. Farmer. 1990. An evaluation of the WOTAN technique for inferring oceanic wind from underwater sound. *Journal of Atmospheric and Oceanic Technology* 7:576–595, http://dx.doi.org/10.1175/1520-0426(1990)007<0576:AEOTWT>2.0.CO;2.

**AUTHORS.** **Jie Yang** (jieyang@apl.washington.edu) is Senior Physicist, Applied Physics Laboratory, University of Washington, Seattle, WA, USA. **Stephen C. Riser** is Professor, School of Oceanography, University of Washington, Seattle, WA, USA. **Jeffrey A. Nystuen** is retired from the Applied Physics Laboratory, University of Washington, Seattle, WA, USA. **William E. Asher** is Senior Principal Oceanographer and **Andrew T. Jessup** is Senior Principal Oceanographer, both at the Applied Physics Laboratory, University of Washington, Seattle, WA, USA.